All-Solution-Processed Transparent Thin Film Transistor and Its Application to Liquid Crystals Driving

Kwang-Ho Lee, Sang-Mook Kim, Huisu Jeong, Yusin Pak, Hui Song, Jeongpil Park, Keon-Hee Lim, Jae-Hoon Kim, Youn Sang Kim, Heung Cho Ko, Il Keun Kwon, and Gun-Young Jung**

Transparent conductive electrodes (TCEs) are widely used in organic light-emitting diodes (OLEDs), liquid crystal displays (LCDs), and organic solar cells. In these devices, indium tin oxide (ITO) has been commonly used as a transparent electrode. The ITO electrode has many merits such as optical transparency, electrical conductivity and environmental stability. With the rapid growth of the display industry, the demand for transparent electrodes has increased dramatically. Accordingly, the exhaustion of the world's indium supply has become an important issue, and the growth of industrial demand has stimulated the rationing of rare-earth metal resources. Therefore, many alternatives to ITO have been developed for use as transparent electrodes, including transparent metal oxides,[1] carbon nanotubes (CNTs),[2] conducting polymers[3] and graphene.[4] However, these alternative materials cannot fulfill all requirements such as high transparency, high electrical conductivity, uniform conductance and high adhesion to substrates. Moreover, most commercial transparent electrodes are produced by vacuum deposition systems, which are not suitable for continuous, i.e., roll-to-roll (R2R), processing, which is the fabrication strategy being pursued to develop next-generation flexible electronics. As alternative processes, metal nanoparticles solution spreading on top of a polymer template has raised an interest due to its ability to produce electrodes without using the costly high-vacuum equipment.

Metal grid electrodes, in which incident light propagates through the gaps between metal lines, have also been explored as transparent and bendable electrodes that do not exhibit losses in conductivity or transmittance; gold (Au) and silver (Ag) grids have been fabricated using a metal nanoparticles (NPs) solution through the self-assembly phenomenon[5] and evaporative lithography,[6] respectively. Silver nanowire-networked films have also been explored as transparent and flexible electrodes in organic light-emitting diodes (OLEDs).[7]

With advances in the development of transparent electrodes, the production of transparent displays may be feasible by using transparent thin film transistors (TTFTs) as the driving units. Im et al.[8] and Riedl et al.[9] demonstrated transparent active matrix and single TTFT OLEDs operated by transparent metal oxide (i.e., ZnO, ZTO) transistors, in which ITO or metal oxide electrodes employed as transparent contact electrodes were deposited by high-vacuum deposition systems, which are not suitable for continuous processing.

In this communication, we discuss the all-solution-processable fabrication of transparent transistors based on transparent metal grid source-drain electrodes and their control over liquid crystals alignment (TFT-LCDs), demonstrating their potential for integration into future transparent displays. The suggested printing and solution-processing methods allow for a continuous process, which is advantageous for achieving simple, low-cost and high-throughput production without the need for costly high-vacuum equipments.

Figure 1 presents a schematic flow of the entire fabrication process for transparent Ag grid electrodes. A hard PDMS (*h*-PDMS) stamp with orthogonal grid features was produced as detailed in a previous study[10] to prevent deformation and distortion. The *h*-PDMS solution was spin-coated (30 μm) and cured on top of a silicon master mold defined by photolithography. Then, a soft PDMS (*s*-PDMS) solution was spin-coated on top of the *h*-PDMS to a thickness of 10 mm. After peeling the *h*-PDMS off the master stamp, orthogonal grid features with a line width of 3 μm and a 30 μm gap size were transferred to the *h*-PDMS, which exhibited both flexibility and hardness. The *s*-PDMS was used as a pressure or stimulation absorber, enabling conformal contact to substrates. The size of

K.-H. Lee, H. Jeong, Y. Pak, H. Song, J. Park, Prof. G.-Y. Jung, Prof. H. C. Ko
School of Materials Science and Engineering
Department of Nanobio Materials and Electronics
Gwangju Institute of Science and Technology (GIST)
123 Cheomdan-gwagiro (Oryong-dong)
Buk-gu, Gwangju 500-712, Republic of Korea
E-mail: gyjung@gist.ac.kr
Dr. S.-M. Kim
Korea Photonics Technology Institute (KOPTI)
ChumDan 4-ro 5, Buk-gu, Gwangju 500-779, Republic of Korea
K.-H. Lim, Prof. Y. S. Kim
Department of Nano Science and Technology
Graduate School of Convergence Science and Technology
Seoul National University
Seoul 151-744, Republic of Korea
Advanced Institute of Convergence Technology
864-1 Iui-dong, Yeongtong-gu, Suwon-si,
Gyeonggi-do 443-72, Republic of Korea
Prof. J.-H. Kim
Department of Electronic Engineering
Hanyang University
Seoul 133-791, Republic of Korea
Prof. I. K. Kwon
Department of Maxillofacial Biomedical Engineering & Institute of Oral Biology, School of Dentistry
Kyung Hee University
Seoul 130-701, Republic of Korea
E-mail:kwo ni@khu.ac.kr

DOI:10. 1002/adma.201300084

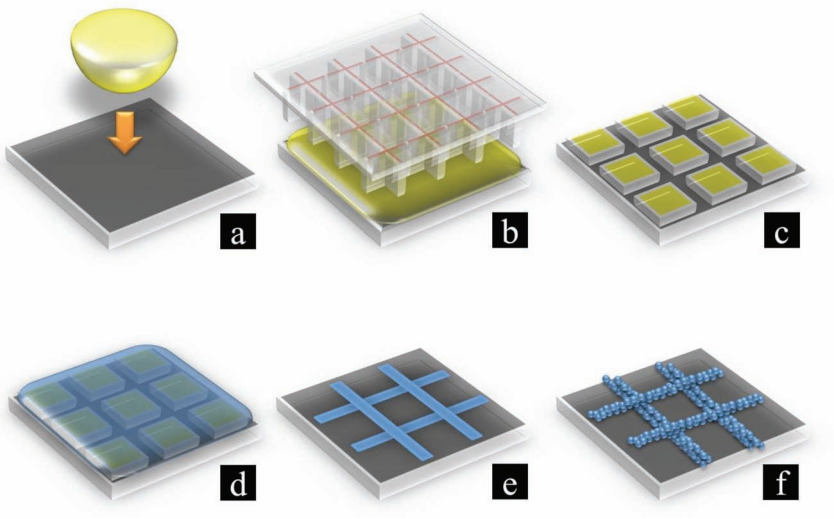

Figure 1. An experimental scheme for the fabrication of Ag grid electrodes: (a) SU-8 resist dropping, (b) *h*-PDMS stamping, (c) reverse printing of polymer template after detachment of the stamp, (d) spin-coating of Ag NPs solution, (e) stripping of the polymer template and (f) sintering.

the *h*-PDMS stamp was 2.5 cm × 2.5 cm. A polymer template was produced by imprinting the SU-8 photoresist film sandwiched between the *h*-PDMS stamp and a glass substrate. A diluted Ag NPs solution was then spin-coated on the polymer template and baked on a hotplate to evaporate the solvent. After lift-off, the Ag NPs grid was annealed in an oven not only to burn the organic dispersant but to establish a continuous electrical path through the NPs aggregation.

Figure 2a and b show field-emission scanning electron microscopy (FE-SEM) images of a polymer template with a thickness of 320 nm. The inset image of Figure 2a demonstrates the large-area patternability of the structure, without any residual layer in the imprinted trench regions (Figure 2b). The Ag grid is faithfully reproduced with no observable cracks or vacancies along the wires after sintering (Figure 2c).

Figure 2d shows an AFM image of a part of the Ag grid electrode with a thickness of 150 nm, which shows that the height of the wire edges is higher than that of the central region according to the surface profile. This uneven surface profile may be generated by capillary action along the microchannels. When the Ag NPs solution is confined in the microchannels, the solution moves upward at the edges because the cohesive force between molecules of the solution is weaker than the adhesion force between the solution and polymer template, generating a concave meniscus. Preliminary experiments reveal that thicker polymer templates generate thicker Ag wires, which exhibit lower sheet resistance but a more prominent edge profile. However, the transmittance remains nearly constant regardless of the thickness of the Ag wire because the same aperture area is retained (see Supporting Information S1).

Ag grid electrodes were fabricated on top of both glass and flexible PET substrates. The inset images in Figure 2e and f show the substrates with invisible Ag grid electrodes measuring 4 cm^2 in area; the glass- and PET-based electrodes show averaged transmittances of 79.6% and 69.4% in the visible range (from 400 to 800 nm), respectively. The loss of transmittance through the Ag grid electrodes is ~13% in both cases. The sheet resistance is also an important parameter in evaluating the performance of transparent electrodes; in this study, values of 6.13 ± 0.12 and 7.95 ± 0.12 Ω/□ are measured for the rigid and flexible transparent electrodes, respectively. It should be noted that neither the transmittance nor the sheet resistance of the Ag grid electrode are changed over a period of four months of storage in air.

A bending test was performed to evaluate the stability of the conductance of the Ag grid electrode on the flexible PET substrate under mechanical stress. Figure 2g plots R/R_o as a function of 1000 cycles of bending (radius ≤ 12 mm), where R_o is the initial resistance; values of 108.1 and 8.4 Ω are measured for the ITO PET and the Ag grid PET, respectively. R_o and R were automatically measured before and after the bending test between two electrical probe lines with a spacing of 2 cm located at both substrate edges. The R/R_o of the Ag grid PET remains constant over 1000 bending cycles, but that of the ITO PET increases five-fold due to the cracking of the ITO. A taping test also demonstrates that the Ag grid electrode is firmly adhered to the substrates. In addition, our Ag grid flexible PET electrode was electrically connected to a light-emitting diode through a crocodile clip, and the electrical conductance of the Ag grid electrode was measured by monitoring the variation in the light output intensity during bending. The variation with bending is not noticeable in the case of the Ag grid PET electrode, as shown in Figure 2h (flat) and Figure 2i (bent). In comparison, in the case of the ITO PET electrode, the light output intensity is sensitive to bending; in fact, the diode shows almost no intensity when it is bent, and the intensity is restored when the mechanical strain is released (see the video files in supporting information S2).

To evaluate the versatility of the Ag grid electrode, transparent thin film transistors (TTFTs) were employed. Conventional silicon-based TFTs are not suitable driving units for transparent displays because the materials used as semiconductors and electrodes are not transparent. Therefore, transparent metal oxide-based materials such as ITO, IZO, ZnO, IGZO and Al_2O_3 have been investigated for use in TFTs as electrodes, gate dielectrics and semiconductors.[8,11,12] However, these materials are deposited using high-vacuum deposition systems.

In this study, we attempt to fabricate all-solution-processable TTFTs, which have not yet been demonstrated to the best of our knowledge. The TTFTs have a configuration of bottom gate-top contact Ag grid source/drain electrodes with a 5000 μm channel width and a 50 μm channel length, as shown in **Figure 3**a. A fluorine-doped tin oxide (FTO) glass is used as a common gate electrode. The FTO glass was coated with methyl siloxane-based spin on glass (SOG), which has been widely used as a gate dielectric layer in organic[13,14] and inorganic transistors[15] due to

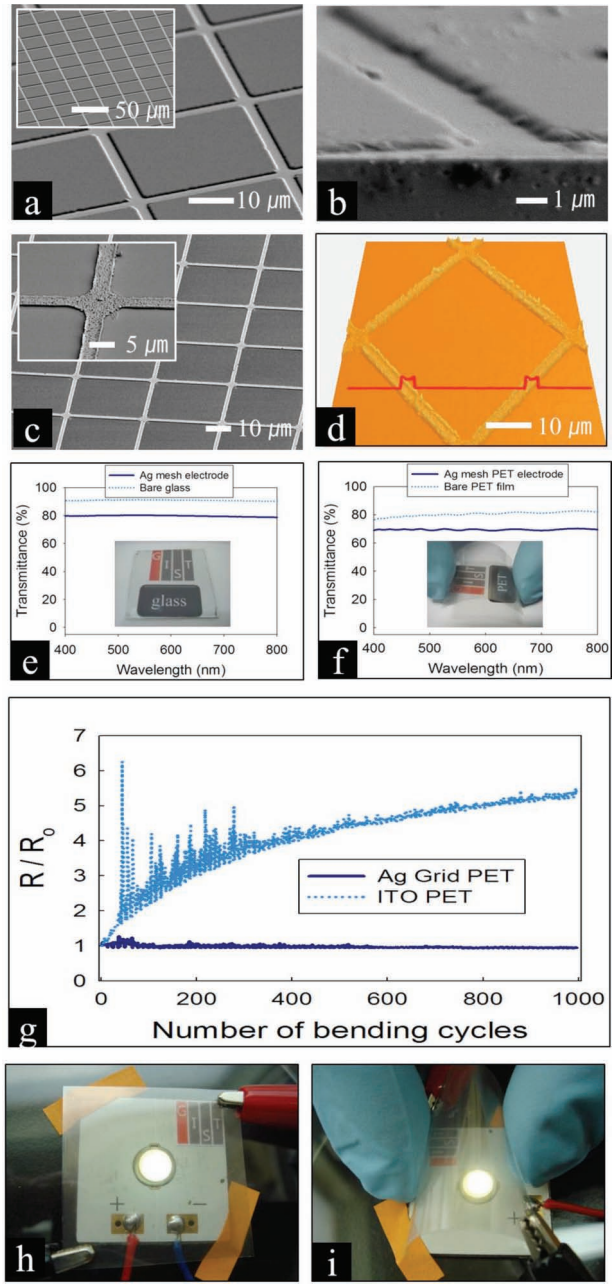

Figure 2. (a) An SEM image of the printed SU-8 template. The inset shows faithful printing over a large area. (b) A tilted SEM image of a printed trench with no residual layer. (c) The Ag grid electrode after sintering, showing a line width of 3 μm and 30 μm spacing. The inset shows a magnified image of a junction with rough edges along the wires, further resolved by the AFM surface profile in (d). Optical transmittance of the Ag grid electrode with respect to that of bare glass (e) and flexible PET film (f). (g) The variation of resistance with the bending cycles. Snapshots of the light output from an LED through the electrically connected flexible transparent Ag grid electrode PET film in planar (h) and bent (i) states.

its solution processability and thermal stability. As an n-type semiconductor, amorphous zinc tin oxide (ZTO) was adopted owing to its sol-gel processability, high transparency and moderate electrical characteristics. The ZTO-based transistors exhibited mobilities and on-off ratios in the range of 1.1 ~ 14.11 cm^2/Vs and 10^5~10^8, respectively.[16–19]

We investigated the effect of the Zn/Sn molar ratio of the ZTO precursor solution on the electrical properties of ZTO-based transistors with the same configuration as shown in Figure 3a but with electron-beam-evaporated aluminum source/drain top contacts. The best field-effect mobility (5.87 cm^2/Vs) and on-off ratio (3.3×10^8) are obtained from a precursor solution with a Zn:Sn molar ratio of 3:7 (see supporting information S3). A thermally annealed ZTO film was characterized by X-ray diffraction (XRD), exhibiting an amorphous phase with a broad diffraction profile without any peaks (see supporting information S4). Previous studies have reported broad and small peaks assigned to ZnO crystal planes in amorphous ZTO films.[16,18] The discrepancy is ascribed to the Sn concentration in ZTO films. Frutos et al. reported a phase transition in ZnO films with different Sn concentrations (by target weight%) ranging from 0.1% to 10% using XRD measurements.[20] The ZnO film with 0.1% Sn shows peaks from the pure ZnO crystal planes. The crystallinity of ZnO disappears with an increase in the Sn concentration to 10%. Due to the high concentration of Sn (Sn mol% = 0.7 defined by Sn/Sn+Zn) in our sol-gel processed ZTO film, the crystalline peaks disappear and the film becomes amorphous, consistent with a previously reported result.[21] Bae et al. reported a mobility of 14.11 cm^2/Vs and an on/off ratio greater than 10^8 from solution-processed amorphous ZTO transistors with aluminum (Al) top contacts.[19]

The optical transmittance of a TTFT composed of FTO glass, a 730 nm thick SOG film, a 20 nm thick ZTO layer and 150 nm thick Ag grid source/drain electrodes was measured and compared with the transmittances of FTO glass samples coated with each respective film, as shown in Figure 3b. The average transmittance of the FTO glass in the visible range is 73.4%. Interestingly, a notable improvement in transparency is observed in the SOG sample (80.4%), presumably due to the better refractive index matching at the interfaces of FTO (n = 1.85)/SOG (n = 1.39)/air (n = 1.0) than that at the FTO/air interface, which reduced the significant total internal reflection that occurs at the interface between two media with a large difference in their refractive indices.[22]

Moreover, the rough surface of the FTO substrate (rms roughness: 22.62 nm over 4 μm^2) results in a decrease in transmittance due to stronger light scattering on the rough surface. However, the SOG film covering the rough FTO glass surface makes the surface smooth, with rms roughness value of 0.56 nm over the same scanning area, resulting in an improved transmittance compared to that of the FTO substrate. Pinto et al. reported the same effect of surface roughness on transmittance.[23] The FTO substrate with the Ag grid source/drain electrodes shows 64.7% transparency (approximately 9% loss of light compared to the reference), but the optical transmittance of the entire TTFT device (73.8%) is restored to that of the bare FTO substrate over the entire visible range. The optical images on the right side of Figure 3b demonstrate the transparency of each layer as well as that of the transparent TTFT device. AFM measurement of the ZTO film on top of the SOG/FTO substrate shows a smooth surface with an rms roughness of 0.55 nm, which provides good interfaces for both the source and drain electrode contacts. AFM images of the

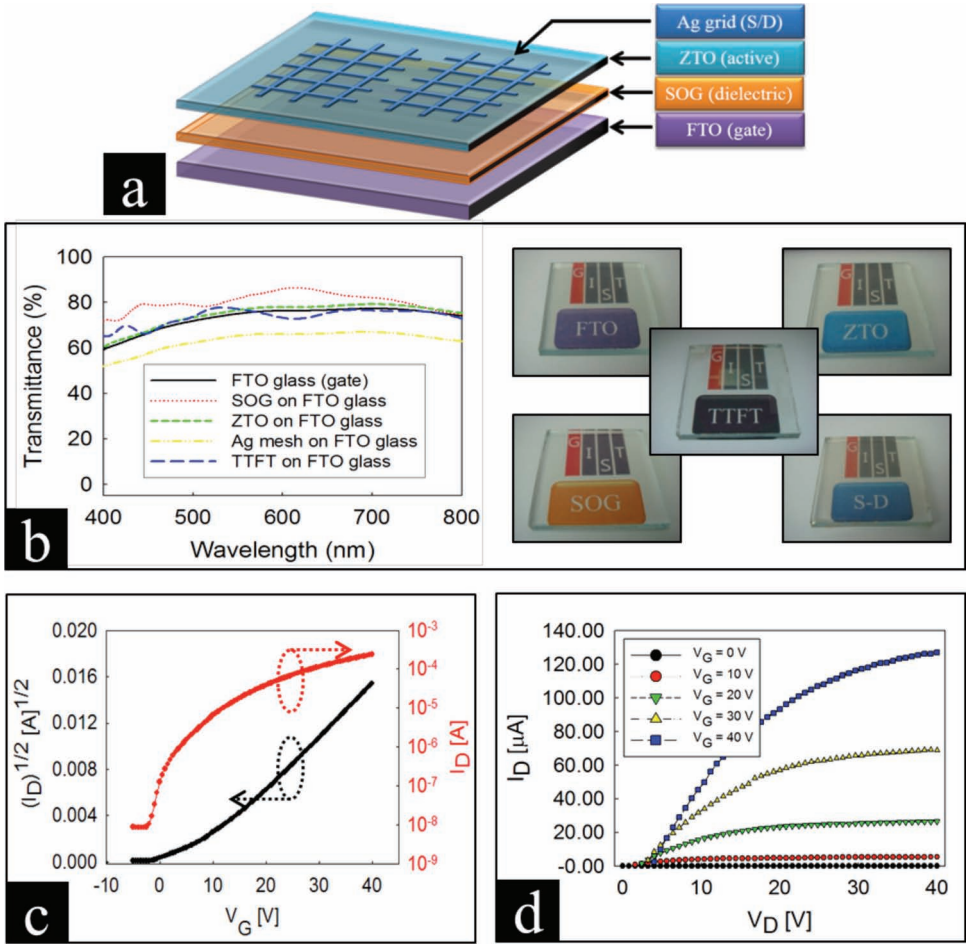

Figure 3. (a) A schematic of a bottom gate-top contact TTFT with Ag grid source/drain electrodes. (b) Comparison of optical transmittances of the entire TTFT, the functional gate dielectric, active materials and Ag grid electrodes with reference to that of the bare FTO substrate and the corresponding photographs demonstrating the transparency of each layer. (c) The transfer characteristics at $V_D = 40$ V and (d) output curves of a TTFT with a channel length of 50 μm and a channel width of 5000 μm.

FTO, SOG and ZTO surfaces are shown in supporting information S5.

Figure 3c shows the transfer characteristics of our TTFT at $V_D = 40$ V as a function of V_G values of –5 ~ 40 V. The results indicate the *n*-type transistor performance of the semiconducting ZTO, with a charge carrier mobility of 1.27 cm^2/Vs, a threshold voltage of 1.7 V and an on-off ratio of 2.8×10^4. These values are inferior to those of the aforementioned transistors with the electron-beam evaporated Al source/drain contacts, mainly due to the higher work function of Ag compared with that of Al.[24] Figure 3d shows a typical transistor output curve of the TTFT at V_G ranging from 0 to 40 V.

We demonstrated the switching properties of a twisted nematic (TN) mode liquid crystal (LC) cell, which was driven by our single TTFT to demonstrate its potential use in the field of transparent displays. The entire LC system is schematically shown in **Figure 4**a, in which the LC cell is placed on top of the TTFT. The source electrode of the TTFT is connected to the bottom electrode in the LC cell, with the top electrode of the LC cell grounded, as depicted in the electric circuit diagram in Figure 4a. A rectangular pulse was applied to the gate electrode from 0 to 20 V at 0.25 Hz with a constant drain voltage of 10 V. The TN-mode LC cell was fabricated in normally white mode, which yields the maximum transmittance under zero bias due to the waveguiding properties of the continuous 90° twisted liquid crystals, which can be reoriented perpendicular to the substrate above a certain electric field. Under these conditions, polarized incident light cannot propagate through the analyzer of the LC cell, leading to a minimum transmittance. At zero gate bias, the underlying 'GIST' logo is clearly seen through both the TTFT and the LC cell, as shown in Figure 4b. When a gate voltage is applied over the threshold voltage of the TTFT, the intensity of propagating light gradually decreased with increasing gate bias due to the LC reorientation, as shown in Figure 4c. When the LC molecules are aligned parallel to the electric field at a gate bias of 20 V, the underlying GIST logo is invisible. The LC cell can be switched between a white and a black state by controlling the gate bias (V_G) of the TTFT, as demonstrated in a video file (see supporting information S6). The transmittance of the LC system was measured by using a

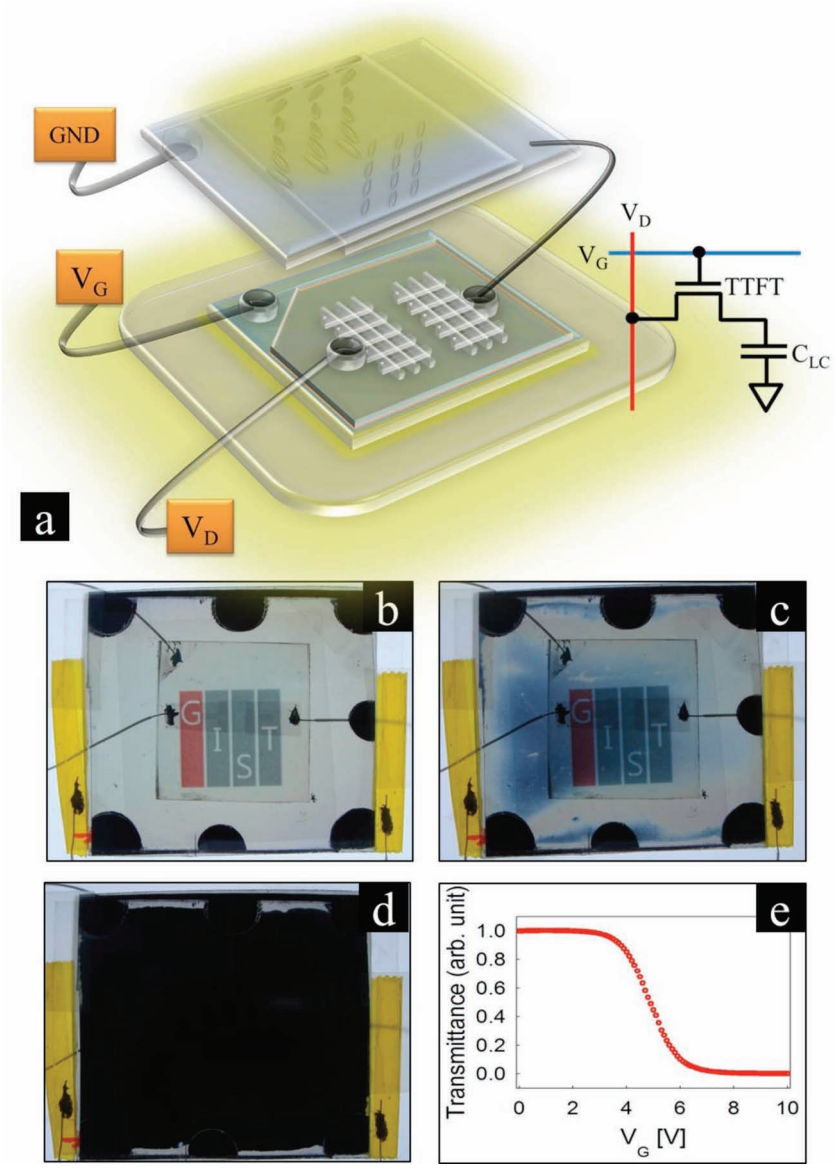

Figure 4. (a) A schematic of a liquid crystal (LC) cell placed on top of a TTFT cell functioning as a driving unit to control the LC orientation and the corresponding electric circuit diagram. Snapshots of (b) the 'white' deactivated state at $V_D = 10$ V and $V_G = 0$ V, (c) the transition state at $V_D = 10$ V when $V_G > V_{th}$ and (d) the 'black' activated state at $V_D = 10$ V, $V_G = 20$ V. The LC cell can be switched between the two states at a frequency of 0.25 Hz. (e) Transmittance of the LC cell with crossed polarizers as a function of the gate voltage of the TTFT.

He-Ne laser ($\lambda = 633$ nm) with a laser spot size of 1 mm. The threshold voltage of this system is 3.4 V, and the transmittance is saturated at 7.7 V (Figure 4e). The response time measurement of our LC cell reveals 20.12 ms for turn-on and 1.59 ms for turn-off, respectively.

In summary, we have fabricated all-solution-processed TTFTs with Ag grid source/drain electrodes, which allow continuous processing without the need for costly high-vacuum systems. Ag grid electrodes with a reasonable transmittance of 80% in the visible range and a sheet resistance of 6.13 ± 0.12 Ω/□ are fabricated by printing and subsequent Ag NPs solution coating. Bending and taping tests showed that the electrodes are mechanically and electrically stable. The TTFTs show a typical *n*-type transistor performance; a mobility of 1.27 cm^2/Vs, a threshold voltage of 1.7 V and an on-off ratio of 2.8 × 10^4. The transmittance of a TTFT utilized as a driving unit to switch twisted nematic (TN)-mode liquid crystal (LC) cells is similar to that of bare FTO glass over the entire visible range. As such, this study demonstrates the potential of incorporating TTFTs into future transparent displays.

Experimental Section

Polymer template fabrication: The fabrication of h-PDMS stamps was detailed in a previous report.[10] An SU-8 resist (MicroChem, Germany) was diluted with an AZ-1500 thinner (AZ Electronics Materials, Germany) in a ratio of 1:2 by weight. The diluted solution was dropped onto a substrate, and the h-PDMS stamp was then placed on the resist using a contact printer (HTM-500, Hutem) with a pressure of 9.8 kPa. Then, the h-PDMS/SU-8/substrate assembly was baked at 100 °C for 1 min. Reverse patterns were replicated on the SU-8 resist after detaching the h-PDMS stamp.

Ag grid electrode fabrication process: An Ag NPs solution (NPS-J, Harima Chem., Japan, 5 nm particle size on average, dispersed in tetradecane at 60 wt%) was diluted with hexane (Sigma Aldrich, USA) in a ratio of 1:20 by weight, spin-coated on the previously prepared polymer template at 4000 rpm for 30 sec and subsequently baked at 100 °C for 1 min to evaporate the solvent. Finally, the SU-8 resist was removed by soaking in acetone with delicate hand stirring. To connect the Ag NPs electrically, sintering was performed in an oven at 100 °C for 5 h.

TTFT device fabrication: FTO glass substrates (sheet resistance: 8 Ω/□) was purchased from Piklington (TEC-7, Japan) and cleaned with acetone, iso-propyl alcohol (IPA) and deionized (DI) water, successively, in an ultrasonic bath. A siloxane-based SOG (Honeywell 512B, USA) was spin-coated on the FTO glass at 4000 rpm for 40 sec and baked on a hot plate in air at 250 °C for 1 min. Finally, it was fully annealed at 400 °C for 1 h under a N_2 flow rate of 100 sccm. A precursor solution for the ZTO film was formulated by dissolving 0.09 M of zinc acetate (0.17 g, $Zn(CH_3CO_2)_2$, Sigma Aldrich, USA) and 0.21 M of tin (II) chloride (0.4 g, $SnCl_2$: Sigma Aldrich, USA) in 2-methoxyethanol solvent (10 ml). A stabilizing agent of 0.18 M of ethanolamine (0.05 g, $NH_2CH_2CH_2OH$, Sigma Aldrich, USA) was added to the solution to enhance the solubility of the zinc precursor. The solution was stirred sufficiently for 3 h at room temperature and then filtered using a disposable filter (filter size: 0.1 μm) prior to use. The ZTO solution was spin-coated on the SOG/FTO substrate and then annealed inside a furnace at 500 °C for 1 h in air. Ag grid source/drain electrodes were fabricated on top of the ZTO as described.

Supporting Information

Supporting Information is available from the Wiley Online Library or from the author.

Acknowledgements

This work was partially supported by the Basic Science Research Program through the National Research Foundation of Korea (NRF, No. R15-2008-006-03002-0, CLEA, NCRC; 2011-0029414) and the World Class University Program (WCU, No. R31-2008-000-10026-0) at GIST funded by the Ministry of Education, Science and Technology (MEST).

Received: January 7, 2013
Revised: February 25, 2013
Published online: April 22, 2013

[1] S. M. Lee, C. S. Choi, K. C. Choi, H. C. Lee, *Org. Electron.* **2012**, *13*, 1654.
[2] Q. Cao, S. H. Hur, Z. T. Zhu, Y. Sun, C. Wamg, M. A. Meitl, M. Shim, J. A. Rogers, *Adv. Mater.* **2006**, *18*, 304.
[3] M. Vosgueritchian, D. J. Lipomi, Z. Bao, *Adv. Funct. Mater.* **2012**, *22*, 421.
[4] S. Pang, Y. Hernadez, X. Feng, K. Müllen, *Adv. Mater.* **2011**, *23*, 2779.
[5] A. Morag, L. P. Mazor, R. Volinsky, E. Mentovich, S. Richter, R. Jelinek, *Adv. Mater.* **2011**, *23*, 2779.
[6] M. Layani, S. Magdassi, *J. Mater. Chem.* **2011**, *21*, 15378.
[7] X. Y. Zeng, Q. K. Zhang, R. M. Yu. C. Z. Lu, *Adv. Mater.* **2010**, *22*, 4484.
[8] S. H. K. Park, C. S. Hwang, M. Ryu, S. Yang, C. Byun, J. Shin, J. I. Lee, K. Lee, M. S. Oh, S. Im, *Adv. Mater.* **2009**, *21*, 678.
[9] P. Görrm, M. Sander, J. Meyer, M. Kröger, E. Becker, H. H. Johannes, W. Kowwalsky, T. Riedl, *Adv. Mater.* **2006**, *18*, 738.
[10] T. W. Odom, J. C. Love, D. B. Wolfe, K. E. Paul, G. M. Whitesides, *Langmuir* **2002**, *18*, 5314.
[11] A. Suresh, J. F. Muth, *Appl. Phys. Lett.* **2008**, *92*, 033502.
[12] S. Ju, A. Facchetti, Y. Xuan, J. Liu, F. Ishikawa, P. Ye, C. Zhou, T. B. Marks, D. B. Janes, *Nat. Nanotechnol.* **2007**, *2*, 378.
[13] K. K. Han, S. Y. Park, M. J. Kim, H. H. Lee, *Appl. Phys. Lett.* **2005**, *87*, 253502.
[14] J. H. Kwon, J. H. Seo, S. I. Shin, K. H. Kim, D. H. Choi, I. B. Kang, H. Kang, B. K. Kwon, *IEEE. T. Electron Dev.* **2008**, *55*, 500.
[15] J. H. Kwon, J. H. Seo, S. I. Shin, B. K. Ju, *J. Phys. D: Appl. Phys.* **2009**, *42*, 065105.
[16] S. Jeong, Y. Jeong, J. Moon, *J. Phys. Chem. C.* **2008**, *20*, 11082.
[17] S. K. Park, Y. H. Kim, H. S. Kim, J. I. Han, *Solid-State Lett.* **2009**, *12*, H256.
[18] Y. J. Chang, D. H. Lee, G. S. Herman, C. H. Chang, *Solid-State Lett.* **2007**, *10*, H135.
[19] S. J. Seo, C. G. Choi, Y. H. Hwang, B. S. Bae, *J. Phys. D: Appl. Phys.* **2009**, *42*, 035106.
[20] E. L. Ponce, J. L. Costa-Krämer, M. S. Martin-Gonzalez, F. Briones, J. F. Fernandez, A. C. Caballerero, M. Villegas, J. Frutos, *Phys. Stat. Sol. A* **2006**, *6*, 1383.
[21] J. H. Ko, I. H. Kim, K. S. Lee, T. S. Lee, B. Cheong, W. M. Kim, *Appl. Surf. Sci.* **2007**, *253*, 7398.
[22] F. L. Pedrotti, L. S. Pedrotti, in *Introduction to Optics*, Vol. *2*, *Prentice Hall* **1993**, 38.
[23] A. Larena, F. Millan, G. Perez, G. Pinto, *Appl. Surf. Sci.* **2002**, *187*, 339.
[24] L. Solymar, D. Walsh, in *Electrical Properties of Materials*, Vol. *8*, Oxford University Press. **2010**, 172.